WAVES IN RANDOM AND COMPLEX MEDIA
https://doi.org/10.1080/17455030.2023.2166147

Taylor & Francis
Taylor & Francis Group

Optical properties of Mandelbrot quantum dots: does fractality have an essential effect?

D. Haji Taghi Tehrani [a], Abdolreza Rasouli Kenari[b] and M. Solaimani [a]

[a]Department of Physics, Faculty of Mechanical engineering, Qom University of Technology, Qom, Iran;
[b]Faculty of Electrical and Computer Engineering, Qom University of Technology, Qom, Iran

ABSTRACT
The optical properties of two-dimensional $Al_xGa_{1-x}As$ (2D) Mandelbrot quantum dots have been studied by utilizing the density matrix approach. We try to address the question: Does fractality have an essential effect? Two generation values *f* and *m* are considered. For this purpose, we have solved the corresponding 2D Schrodinger equation using the finite difference method. Then, the effect of the fractality order, system size, and the composition parameter *x* on the energy eigenvalues, dipole matrix elements, and the absorption coefficient was considered. We have also described the procedure of numerical creating the Mandelbrot quantum dot potential profile.

ARTICLE HISTORY
Received 21 December 2021
Accepted 2 January 2023

KEYWORDS
Mandelbrot quantum dots; 2D Schrodinger equations; intersubband optical absorption coefficient

1. Introduction

During the last years, quantum dots have attracted much attention due to their similarities to natural atoms, and thus they are called artificial atoms. Unlike the natural atoms, the interband and intersubband transitions can more easily be regulated and through changing the heterostructure geometry, obtaining the desired optical properties is now possible. It is well-known that the size and shape of a quantum structure can have a considerable influence on the physical properties of a typical system [1]. For example, size effects on transition energies [2], size-dependent optical properties [3], size-dependent photoluminescence [4], etc. have thus far been considered. Also, core–shell-shell quantum dots [5], quantum dot superlattice [6], tapered tetrahedral semiconductor nanocrystals [7], Y-shaped quantum dots [8], T-shaped quantum dots [9], pyramid-shaped quantum dots [10], lens-shaped quantum dots [11], conical quantum dots [12], cylindrical quantum dots [13], spherical quantum dots[14], cubic quantum dots [15], etc. are investigated to obtain the optimum quantum dot shape.

However, the real experimental structures such as nano-flowers branched nanowires, and nano-trees [16], which have not conventional simple geometries as mentioned above, indicate that we must try to study more complicated realistic systems such as quantum fractals. Fractals are usually defined using the repetition of similar patterns at ever-diminishing scales. As a result, they are some scale invariant systems. They may have irregular shapes that can be built utilizing some 'replacement rules'. Fractals have potential applications in

CONTACT M. Solaimani solaimani @qut.ac.ir; solaimani.mehdi@gmail.com

biological signaling and image processing [17], reservoir engineering [18], forest science [19], etc.

Fabrication of fractal structures on the micrometer scale is nowadays possible using nanoscale anisotropic etching of single-crystalline structures [20] or using a controllable solution-phase hydrothermal method in the nanometer range [21]. So far, different fractal systems such as fractal resonators [22], fractal waveguide arrays [23], fractal Polymers [24], fractal superlattices [25], fractal optical filters [26], fractal optical lattices [27], graphene Cantor-like structures [28], a quantum electron gas in a Sierpinski carpet [29], electronic Sierpiński fractals [30], self-similar potential structures in a graphene monolayer [31], etc. are addressed. Also, some physical properties of fractal-shaped structures such as Anderson transition [32], energy transfer via exciton transport [33], ferromagnetism [34], broadband spectral response [35], etc. have been studied. Among the different physical properties, the intersubband optical properties of Sierpinski triangles and Sierpinski carpets [36], Koch snowflakes [37], Thue-Morse multiple quantum wells [38], Thue-Morse and Fibonacci planar graphene superlattices [39], Fibonacci multiple quantum well systems [40] are now considered using the effective mass and envelop function formalism employing the density matrix approach. However, the intersubband optical properties of Mandelbrot quantum dots are not so far addressed. This fractal geometry is just slightly utilized in physics research.

It is said that: *The Mandelbrot Set is perhaps the most complex object in mathematics, and it is undoubtedly one of the most fascinating and rewarding mathematical objects to explore* [41]. Mandelbrot has first introduced the fractality concept into the Feynman path integral approach to quantum mechanics [42]. Also, Gardi connected the Mandelbrot set and the fractal nature of light [43]. Besides, in Ref. [44], the dynamics of a kicked charged particle traveling in a double-well potential under the influence of a time-varying magnetic field is considered and in some cases, the stroboscopic dynamics reduced to the complex logistic map and provided a physical meaning for the Mandelbrot set.

In the present study, we have considered the electronic and optical properties of AlxGa1-xAs Mandelbrot quantum dots. This work is organized into few sections. In Section 2, we have described the foundations of the research. In Section 3, we have presented the numerical process of Mandelbrot quantum dot generation. In Section 4, the results are discussed. Finally, in the conclusion section, we have given some summary remarks.

2. Formalism

The physical properties of an electron inside a 2D Mandelbrot quantum dot can be obtained employing the following Schrodinger equation,

$$\left[-\frac{\hbar^2}{2m^*}\left(\frac{\partial^2}{\partial x^2}+\frac{\partial^2}{\partial y^2}\right)+V(x,y)\right]\psi(x,y) = E\psi(x,y) \tag{1}$$

where $m*$ and $\hbar$ are the electron effective mass and the Plank constant, respectively. Equation (1) denotes a linear eigenvalue equation utilizing the Dirichlet boundary conditions. We consider a rectangular domain $\Omega = [a_x, b_x] \times [a_y, b_y]$. In the next section, we have will define the Mandelbrot geometrical confining potentials $V(x, y)$. However, some schematic illustrations of the 2D Mandelbrot quantum dot potential shape $V(x, y)$ for some iterations O (first iteration schema, see section 2-1) and M (secone iteration schema, see section 2-2) are presented in Figures 1 and 2. To solve Equation (1) using the finite differ-

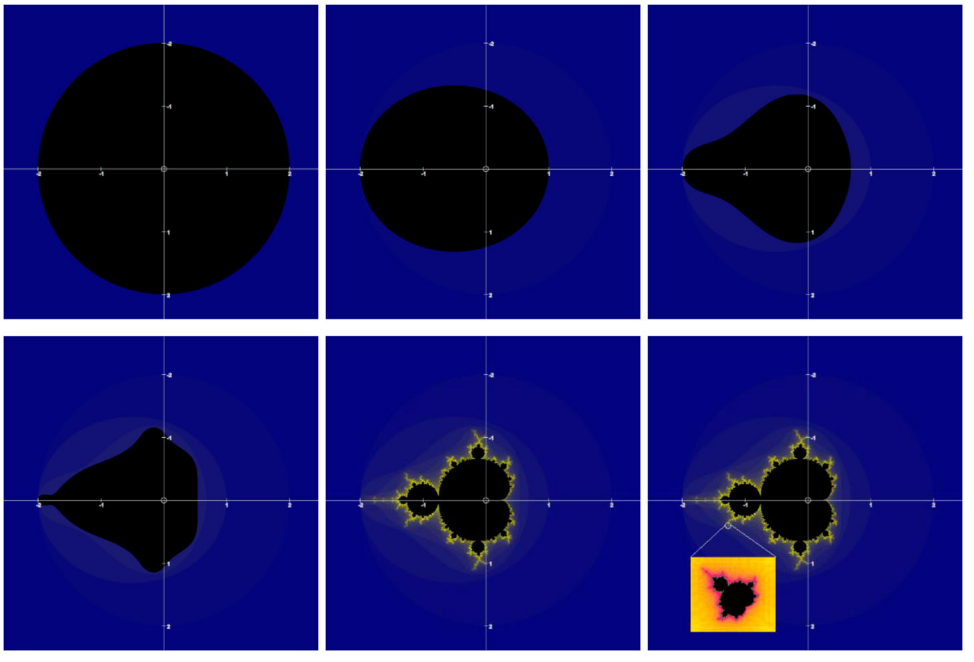

Figure 1. (a) M_S_1 as Circle. (b) M_S_2 as an ellipse. (c) M_S_3. (d) M_S_4. (e) M_S_{50}. (f) Zoom in edges: The resulting shape is the same as the original shape. $m = 2$ for all figures.

ence method, we employed the second derivatives utilizing the 3-point centered difference formula,

$$\frac{f(x+h) - 2f(x) + f(x-h)}{h^2} = f^{(2)}(x) + \frac{h^2}{12} f^4 \tag{2}$$

where $\frac{h^2}{12} f^4$ is the local truncation error (LTE). Using this method we can convert the Equation (1) into a matrix form,

$$H\psi(x,y) = E\psi(x,y) \tag{3}$$

Supposing N_x and N_y number of discretization point along x and y directions we have,

$$\begin{aligned} H\psi(x,y) = &-\frac{\hbar^2}{2m^*} \frac{\psi(x+\Delta x,y) - 2\psi(x,y) + \psi(x-\Delta x,y)}{\Delta x^2} \\ &- \frac{\hbar^2}{2m^*} \frac{\psi(x,y+\Delta y) - 2\psi(x,y) + \psi(x,y-\Delta y)}{\Delta y^2} + V(x,y)\psi(x,y) \end{aligned} \tag{4}$$

then,

$$\begin{aligned} H^{n,m} = &-\frac{\hbar^2}{2m^*} \frac{\psi_{n+1,m} - 2\psi_{n,m} + \psi_{n-1,m}}{\Delta x^2} \\ &- \frac{\hbar^2}{2m^*} \frac{\psi_{n,m+1} - 2\psi_{n,m} + \psi_{n,m-1}}{\Delta y^2} + V(n,m)\psi_{n,m} \end{aligned} \tag{5}$$

Now, H is a $(Nx \times Ny) \times (Nx \times Ny)$ matrix.

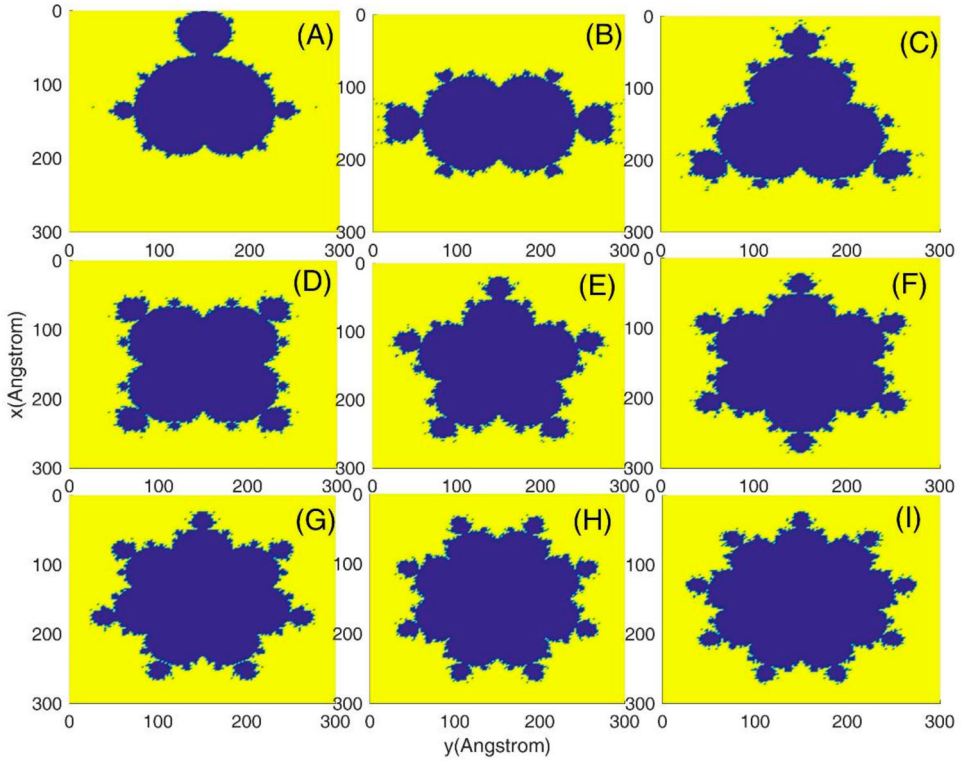

Figure 2. Schematic illustrations of the 2D complete Mandelbrot quantum dot potential shapes for $m = 2$–10 and $f = 10$ in panels (A)–(F).

The linear absorption coefficient for $(E_f - E_i)$ transition can be obtained using [45],

$$\alpha^{(1)}(\omega) = \omega\sqrt{\frac{\mu}{\varepsilon_r}} \times \frac{\sigma_s e^2 |M_{fi}|^2 \hbar\Gamma_{fi}}{(\hbar\omega - \Delta E_{fi})^2 + (\hbar\Gamma_{fi})^2} \tag{6}$$

where ω is the excitation electromagnetic field frequency. σ_s denotes the electron density inside the structure, E_i and E_f represent the quantized energy levels for the initial and final states, respectively. These values are obtained by solving the 2D Schrodinger equation. μ is the permeability and $\Gamma_{fi}(f \neq i)$ is the inverse of relaxation time T_{fi} for states $|f\rangle$ and $|i\rangle$, namely $\Gamma_{fi} = 1/T_{fi}$. Finally, the incident light is x-polarized, i.e. $M_{fi} = \langle\psi_i|x\hat{x}|\psi_j\rangle$ [46].

3. Mandelbrot quantum dot numerical generation process

According to the last section, suppose that a rectangular domain $\Omega = [a_x, b_x] \times [a_y, b_y]$ is discretized by $N_X \times N_Y$ points along x and y directions. Two points set X and Y are defined as Equation (7).

$$\begin{aligned} X &= \{x_i | x_i = a_x + \frac{i}{N_X}(b_x - a_x)\,,\ i = 0, 1, 2, \ldots, N_X\} \\ Y &= \{y_i | y_i = a_Y + \frac{i}{N_Y}(b_y - a_y)\,,\ i = 0, 1, 2, \ldots, N_Y\} \end{aligned} \tag{7}$$

the Mandelbrot geometrical confining potentials $V(x,y)$ are computed as Equation (8) for all $(x,y) \in X \times Y$.

$$V(x,y) = \begin{cases} 1 & if\ (c = x + iy) \in \text{Mandelbrot\_}Set_f \\ 0 & if\ (c = x + iy) \notin \text{Mandelbrot\_}Set_f \end{cases} \tag{8}$$

Where $c = x + iy$ is a complex number with real x and image y. The Mandelbrot_Set$_f$ (M_S$_f$) is the set of complex points defined by Mandelbrot Fractal with f iterations. The M_S$_f$ is a complex fractal over complex function $f(z) = z^m + c$. In fact, for every complex point c; a series of points z_i are calculated as Equation (9).

$$z_{i+1} = {z_i}^m + c\ ,\quad i = 0, 1, 2, \ldots\ , z_0 = 0 \tag{9}$$

The M_S$_f$ with iteration f includes all complex points c, such that $|z_n| \leq 2$. The definition is formalized in Equation (10).

$$M\_S_f = \{c \in \mathbb{C} \mid |z_f| \leq 2\ ,\ z_{i+1} = {z_i}^m\ , z_0 = 0\} \tag{10}$$

For example, for $f = 1$, the $z_1 = c$, because the $z_0 = 0$. So, the M_S$_1$ is all complex points c whose distance to the origin is less than 2 ($|c| \leq 2$). It is obviously a circle with a radius of 2 as shown in Figure 1(a). when $f = 2$, we have $z_2 = {z_1}^m + c = c^m + c$. Here the M_S$_2$ is all c with $|c_2 + c| \leq 2$. Some of M_S$_1$ points fails in new condition and the M_S$_2$ shape is same as an ellipse as shown in Figure 1(b). If the process continues the M_S$_\infty$ will be shrinker and smaller. The M_S$_3$, M_S$_4$, and M_S$_{50}$ are shown in Figure 1(c–e), respectively. The magic of the Mandelbrot Set is when you zoom in final shape edges, the same shape you will see. This pheromone is shown in Figure 1(f).

Algorithm applied to build the $V(x, y)$.

Algorithm – Mandelbrot geometrical confining potentials $V_n(x,y)$
Input: $\Omega = [a_x, b_x] \times [a_y, b_y]$
N_x and N_y: Number of discretization point along x and y directions
f: Number of Iterations
Output: Matrix $V_{Nx \times Ny}$ of 0, 1

```
z = 0
For x = a_x To b_x Step by (b_x – a_x) /N_x
  For y = a_y To b_y Step by (b_y – a_y)/N_y
    Let c = x + iy
    If f ~ = 1
      Let z = 0
    For i = 1 To f
      z = z^m + c
    If (|z| ≤ 2)
      V(x, y) = 1
    Else
      V(x, y) = 0
```

In fact, Matrix $V_{Nx \times Ny}(x,y) = 1$, if point (x, y) is inside the Mandelbrot Set, and is equals 0. Otherwise.

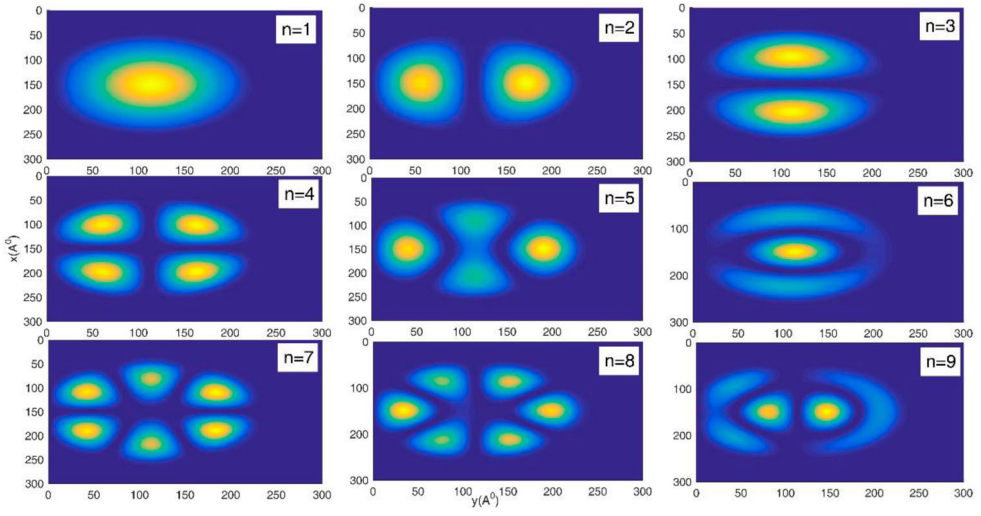

Figure 3. 2D contour plots of the first nine lowest probability densities as a function of position for a Mandelbrot quantum dot with iteration number 1. We have also assumed $x = 0.3$, $m = 2$ and $f = 10$.

4. Results and discussion

In this work, we have considered the optical properties of Mandelbrot $Al_xGa_{1-x}As$ quantum dots. We have restricted ourselves to 2-1 intersubband transitions that are evaluated in the effective mass envelope function approximation. By using different Mandelbrot iterations, we have studied some geometries that its simplest form is a circle inside a square. By solving the corresponding Schrodinger equation we have obtained the energy eigenvalues and related eigenfunctions. In Figures 3–5, three collections of eigenfunctions have been presented. Figure 3 presents the 2D contour plots of the first nine lowest probability densities as a function of position for a Mandelbrot quantum dot with iteration number 1 (see panel (B) of Figure 1 for the corresponding potential profile). Here, it is assumed that $x = 0.3$. Figure 4 is the same as Figure 3 but for iteration number 9, and Figure 5 is the same as Figure 3 but for $x = 0.25$. in Figures 3 and 4, which we have deeper quantum wells inside the Mandelbrot quantum dots, the corresponding eigenfunctions are better localized in the good regions, while in Figure 5 the eigenfunctions have leaked outside of the good region too. This means the potential well is not strong enough to confine the wave function inside deeper potential areas. A direct conclusion is that using the good depth inside the Mandelbrot dot areas, we can manage the probability density distribution throughout the supposed spatial domain. In all panels, the eigenfunctions have a symmetry axis on $x = 150A^0$. These symmetries are inherited from the corresponding potential profiles in Figure 1. Finally, comparing Figures 3–5, we see that the overall shapes of the wave function are, roughly speaking, similar to the corresponding potential profiles in Figure 1. For more illustration purposes, we also provided the Figures 6 and 7.

Figure 8B shows the variation of the energy eigenvalues as a function of the energy level index for 10 different values of the Mandelbrot iteration numbers. We assumed $x = 0.3$ and $L = 300A^0$. In this figure, we can see that by increasing the Mandelbrot iteration level, the energy levels increase. However, the magnitude of the increment in the energy levels

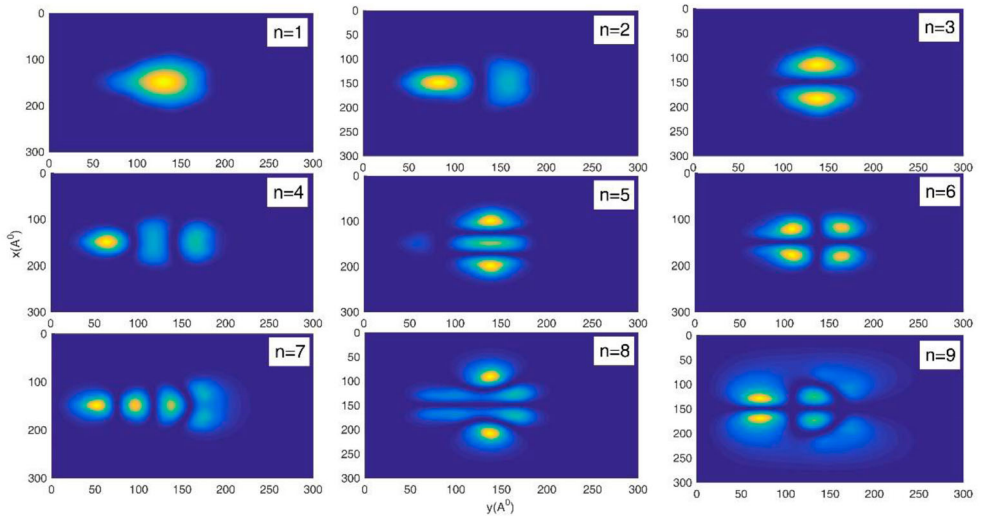

Figure 4. The same as Figure 3 but for iteration number 9, $m = 2$ and $f = 10$.

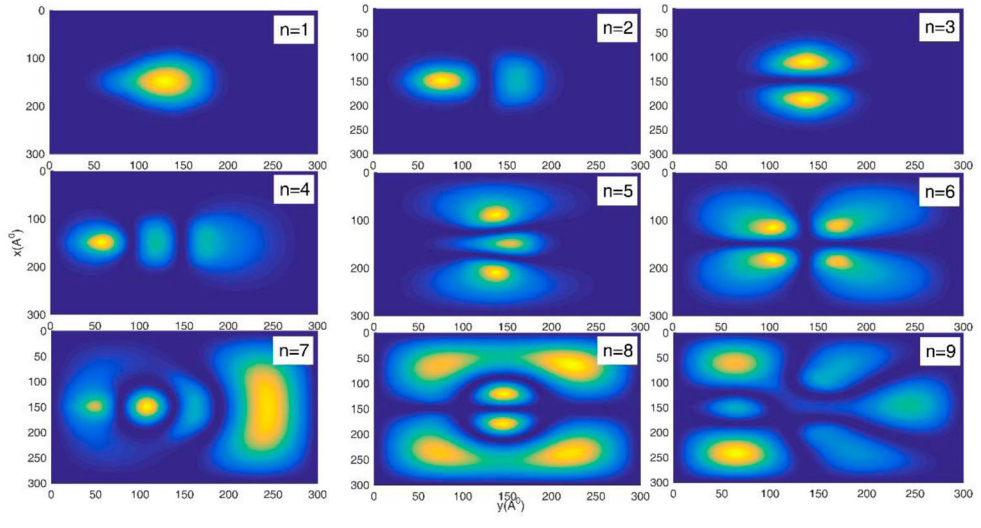

Figure 5. The same as Figure 3 but for $x = 0.25$, $m = 2$ and $f = 10$.

decreases by increasing the Mandelbrot iteration level. This is also because higher levels of Mandelbrot iterations lesser change the potential profile of the quantum dot. Another fact is that the 2-1 intersubband transition increases by increasing the Mandelbrot iteration level. Figure 9B presents the variation of the first six lowest energy eigenvalues as a function of the spatial domain length L. As this figure shows, the energy eigenvalues decrease by increasing the spatial domain length. This is consistent with quantum mechanics concepts. Because, we expect, by increasing the system size, the quantization of the energy levels destroy and a continuum of classical energy produce. Also, in this figure, the energy quantization is more pronounced in systems with smaller sizes. Besides, the 2-1 intersubband transition energy decrease by increasing the system length L.

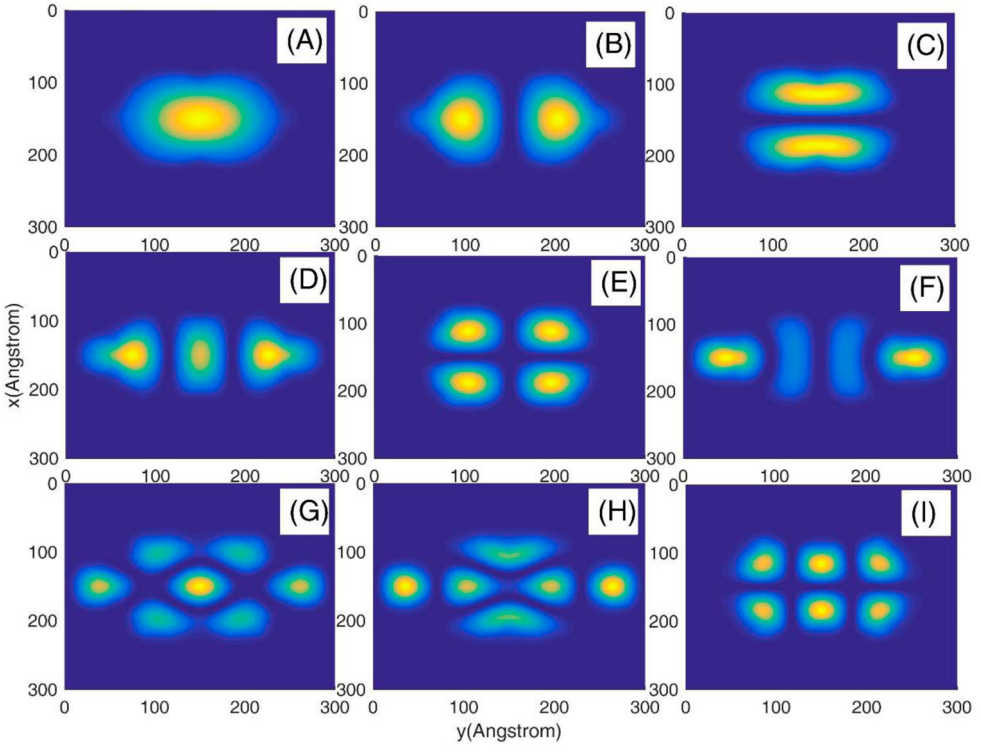

Figure 6. 2D contour plots of the first nine lowest probability densities as a function of position for a complete Mandelbrot quantum dot. We have also assumed $x = 0.3$, $m = 3$ and $f = 10$.

Figure 8 presents the variation of the linear absorption coefficient ($1/m$) as a function of the incident photon energy (eV) for some Mandelbrot quantum dots. The effect of 10 Mandelbrot iteration numbers is compared. Here, it is assumed $x = 0.3$ and $L = 30$ nm. As this figure shows, the system with Mandelbrot iteration 0 has a different behavior from the others. Neglecting this system, as the Mandelbrot iteration level increases the absorption amplitude slightly decreases. This behavior is inherited from Figure 8C. Figure 8C shows the variation of the dipole matrix element μ_{12} as a function of the Mandelbrot iteration number. Also, by increasing the Mandelbrot iteration level the absorption peak positions blueshift. This blue shift is due to increasing the 2-1 intersubband transition by increasing the Mandelbrot iteration level in Figure 8B.

Figure 9A illustrates the variation of the linear absorption coefficient ($1/m$) as a function of the incident photon energy (eV) for some spatial domain lengths $L = 50$, 100, 150, 250, 350, and 450 A^0. It is assumed $x = 0.3$ and nine Mandelbrot iteration numbers. In this figure, as the spatial domain length L increase the absorption coefficient slightly increases (against the effect of the Mandelbrot iteration level). This characteristic is consistent with Figure 9C that shows the variation of the dipole matrix element μ_{12} as a function of the spatial domain length L. Because $|M_{if}|$ is the dominant term as seen also in Equation (6), it generally determines the behavior of the absorption coeffieint [47]. Besides, by increasing the spatial domain length L the absorption peak positions redshift (this is also against the effect of the Mandelbrot iteration level). This redshift is consistent with Figure 9B.

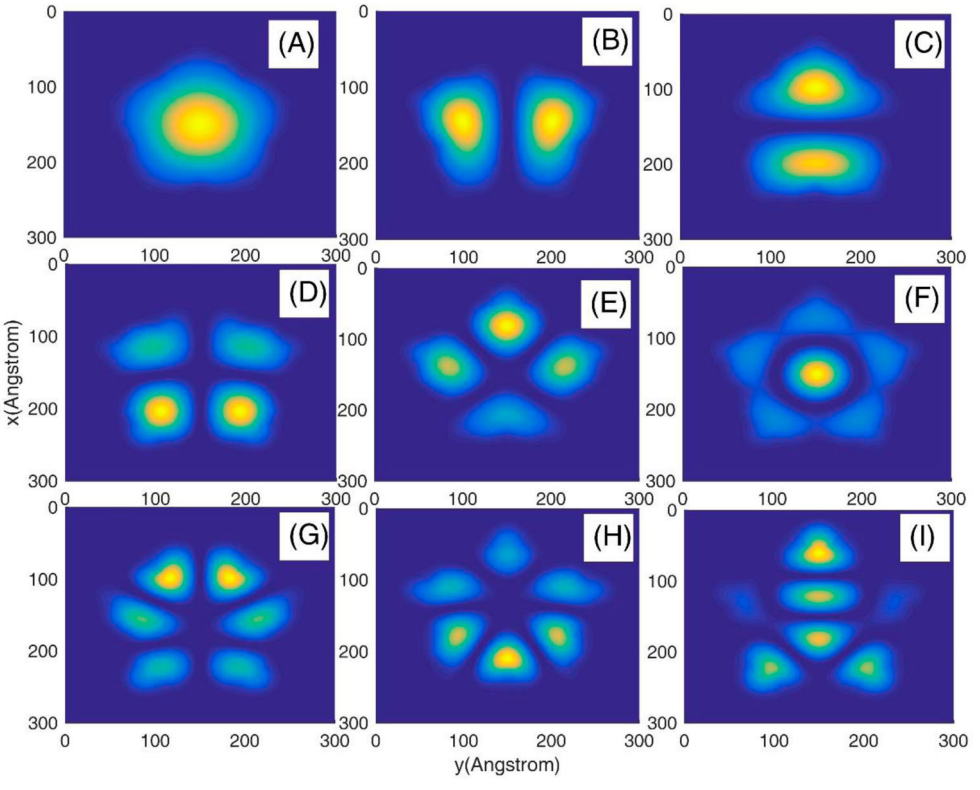

Figure 7. The same as Figure 6 but for $m = 6$ and $f = 10$.

In Figure 10A, we have given the variation of the linear absorption coefficient (1/m) as a function of the incident photon energy (eV) for some complete Mandelbrot quantum dots. Here, the effect of some M is compared. It is assumed $x = 0.3$ and $L = 30$ nm. As this panel shows, iteration M has no considerable effect on the absorption peak position. However, the iteration M $= 9$ is an exception. This behavior is consistent with panel 6C that presents the variation of the dipole matrix element μ_{12} as a function of the M. The behavior of the dipole matrix element is greatly depends on the overlap between the first and second wavefunctions [48]. The wave function shapes and the amount of overlapping is also greatly depend on the QD shape that in our case the QD shape changes irregularly with Mandelbrot iteration. Besides, by increasing M, the absorption peak positions undertake some oscillating red and blueshifts. This characteristic is also agreed with panel 6B that depicts the variation of the energy eigenvalues as a function of the energy level index for some M.

5. Conclusion

In this study, we considered the optical absorption properties of Mandelbrot semiconducting quantum dots. We have shown that by adjusting the internal depth of Mandelbrot dot areas, the probability density distribution throughout the supposed spatial domain can be fine tuned. The energy levels increased by increasing the Mandelbrot iteration level, decreased by increasing the spatial domain length; and increased and then saturated by

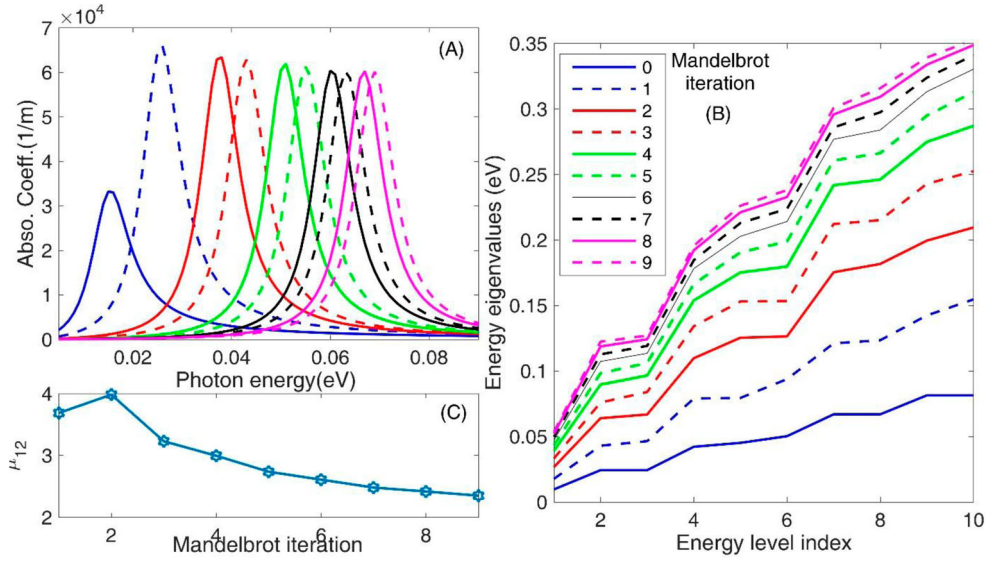

Figure 8. (A) Variation of the linear absorption coefficient ($1/m$) as a function of the incident photon energy (eV) for some Mandelbrot quantum dots. The effect of 10 Mandelbrot iteration numbers is compared. (B) Variation of the energy eigenvalues as a function of the energy level index for 10 different values of the Mandelbrot iteration numbers. (C) Variation of the dipole matrix element μ_{12} as a function of the Mandelbrot iteration number. It is assumed $x = 0.3$ and $L = 30$ nm, $m = 2$.

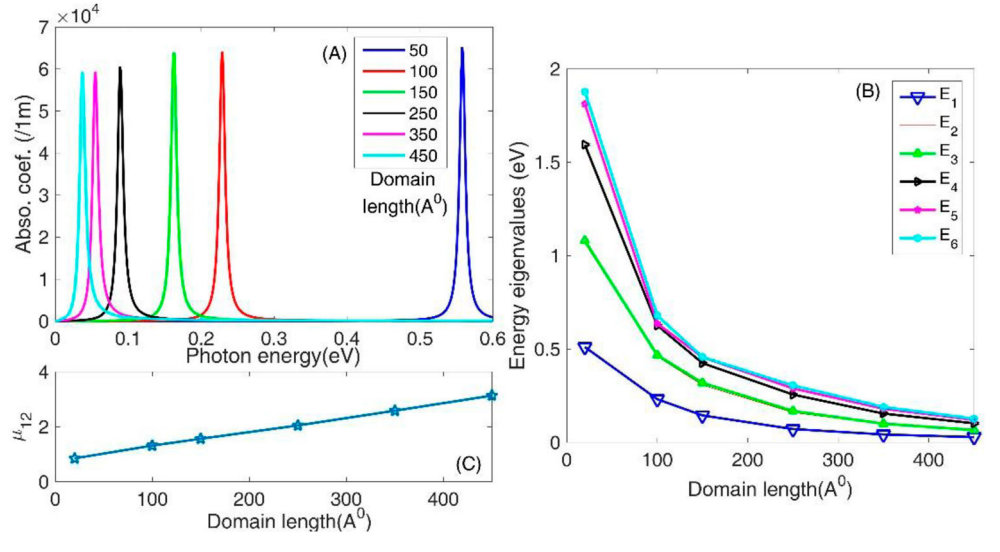

Figure 9. (A) Variation of the linear absorption coefficient ($1/m$) as a function of the incident photon energy (eV) for some spatial domain length $L = 50$, 100, 150, 250, 350, and 450 A^0. (B) Variation of the first six lowest energy eigenvalues as a function of the spatial domain length L. (C) Variation of the dipole matrix element μ_{12} as a function of the spatial domain length L. It is assumed $x = 0.3$, $m = 2$, and nine Mandelbrot iteration numbers.

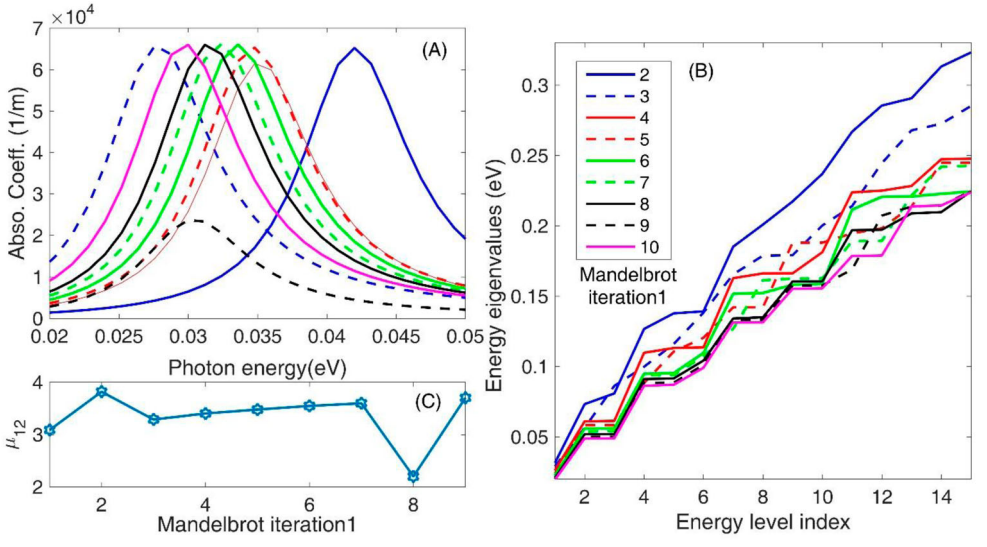

Figure 10. (A) Variation of the linear absorption coefficient (1/*m*) as a function of the incident photon energy (eV) for some complete Mandelbrot quantum dots. The effect of some *m* is compared. (B) Variation of the energy eigenvalues as a function of the energy level index for some M. (C) Variation of the dipole matrix element μ_{12} as a function of the M. It is assumed $x = 0.3$, $f = 10$, and $L = 30$ nm.

increasing the composition parameter *x*. When the Mandelbrot iteration level increased the absorption amplitude slightly decreased and the absorption peak positions blueshifted. As the spatial domain length *L* increased the absorption amplitude slightly increased and the absorption peak positions redshifted. Therefore, the Mandelbrot iteration level and the spatial domain length *L* can be used as fine regulating tools (with opposite effects) to modify the absorption amplitude. Besides, when the composition parameters *x* increased the absorption amplitude decreased and the absorption peak positions blueshifted. However, here, the extent of absorption amplitude variation is more considerable than its changes by Mandelbrot iteration level or the spatial domain length *L*. Finally, to answer the question 'Does fractality have an essential effect on the optical properties on fractal QDs? ', we note that, the Mandelbrot fractality has little effect on the absorption coefficient amplitude, while it can drastically modify the absorption peak position.

Disclosure statement

No potential conflict of interest was reported by the author(s).

ORCID

D. Haji Taghi Tehrani http://orcid.org/0000-0001-6375-6321
M. Solaimani http://orcid.org/0000-0003-4111-4680

References

[1] Popescu I, Hristache M, Ciobanu S-S, et al. Size or shape – what matters most at the nanoscale? Comput Mater Sci. 2019;165:13–22.

[2] Mei G, Carpenter S, Felton LE, et al. Size effects on optical transition energies in CdS_xSe_{1-x} semiconductor nanocrystal glass composites. J Opt Soc Am B. 1992;9:1394–1400.
[3] Zgaren I, Sellami K, Jaziri S. Size-dependent optical properties in II–VI quantum-dot/quantum-well heterostructures. Sens Lett. 2009;7:967–971.
[4] Yu Y, Fan G, Fermi A, et al. Size-dependent photoluminescence efficiency of silicon nanocrystal quantum dots. J Phys Chem C. 2017;121:23240–23248.
[5] Zeiri N, Naifar A, Abdi-Ben Nasrallah S, et al. Theoretical studies on third nonlinear optical susceptibility in CdTe-CdS-ZnS core-shell-shell quantum dots. Photonics Nanostructures – Fundam Appl. 2019;36:100725.
[6] Faleev NN, Honsberg C, Punegov VI. Quantitative analysis of the quantum dot superlattice by high-resolution x-ray diffraction. J Appl Phys. 2013;113:163506.
[7] Na G, li Y, Wang X, et al. Electronic and optical properties of tapered tetrahedral semiconductor nanocrystals. Nanotechnology. 2021;32:295203.
[8] Fang T-F, Wang S-J. Cross correlations and shot noise in a Y-shaped quantum dot. J Phys: Condens Matter. 2007;19:026204.
[9] Wu BH, Cao JC. Interference of conductance and shot noise properties of photon-assisted transport through a T-shaped double quantum dot. Phys Rev B. 2006;73:205318.
[10] Sabaeian M, Shahzadeh M. Self-assembled strained pyramid-shaped InAs/GaAs quantum dots: The effects of wetting layer thickness on discrete and quasi-continuum levels. Physica E. 2014;61:62–68.
[11] Rodrıguez AH, Ramırez HY. Analytical calculation of eigen-energies for lens-shaped quantum dot with finite barriers. Eur Phys J B. 2008;66:235–238.
[12] Melnik RVN, Willatzen M. Bandstructures of conical quantum dots with wetting layers. Nanotechnology. 2004;15:1–8.
[13] Solaimani M, Lavaei L, Aleomraninejad SMA. Optical rectification coefficients of cylindrical quantum dots: rashba spin-orbit interaction effects. J Opt Soc Am B. 2017;34:1989–1993.
[14] Solaimani M, Ghalandari M, Lavaei L. Donor impurity effects on optical properties of GaN/AlN constant total effective radius multishell quantum dots. J Optical Soci America B. 2016;33:420–425.
[15] Boichuk VI, Bilynsky IV, Shakleina IO, et al. Dielectric mismatch in finite barrier cubic quantum dots. Physica E. 2010;43:161–166.
[16] Yao W-T, Yu S-H, Liu S-J, et al. Architectural control syntheses of CdS and CdSe nanoflowers, branched nanowires, and nanotrees via a solvothermal approach in a mixed solution and their photocatalytic property. J Phys Chem B. 2006;110:11704–11710.
[17] Kumar DK, Arjunan SP, Aliahmad B. Fractals: applications in biological signalling and image processing. London: CRC Press; 2017.
[18] Hardy HH, Beier RA. Fractals in reservoir engineering. Singapore: World Scientific; 1994.
[19] Lorimer ND. The fractal forest: fractal geometry and applications in forest science Vol. 170. St. Paul (MN): North Central Forest Experiment Station, Forest Service, US Department of Agriculture; 1994.
[20] Berenschot EJW, Jansen HV, Tas NR. Fabrication of 3D fractal structures using nanoscale anisotropic etching of single crystalline silicon. J Micromech Microeng. 2013;23:055024.
[21] Peng Q, Dong Y, Deng Z, et al. Selective synthesis and characterization of CdSe nanorods and fractal nanocrystals. Inorg Chem. 2002;41:5249–5254.
[22] Russ S, Sapoval B, Haeberle O. Irregular and fractal resonators with neumann boundary conditions: density of states and localization. Phys Rev E. 1997;55:1413–1421.
[23] Jia S, Fleischer JW. Nonlinear light propagation in fractal waveguide arrays. Opt Expr. 2010;18:14409–14415.
[24] Mantela M, Lambropoulos K, Theodorakou M, et al. Quasi-periodic and fractal polymers: energy structure and carrier transfer. Materials (Basel). 2019;12:2177.
[25] Aubert H, Jaggard DL. Fractal superlattices and their wavelet analyses. Opt Commun. 1998;149:207–212.

[26] Solaimani M, Ghalandari M, Nejati M. Optical filters based on fixed length Thue–Morse plasma-dielectric photonic band multilayers: comparing two, three, and four materials systems. AIP Adv. 2021;11:025309.
[27] Singh K, Saha K, Parameswaran SA, et al. Fibonacci optical lattices for tunable quantum quasicrystals. Phys Rev A. 2015;92:063426.
[28] García-Cervantes H, Gaggero-Sager LM, Díaz-Guerrero DS, et al. Self-similar conductance patterns in graphene cantor-like structures. Sci Rep. 2017;7:1–10.
[29] van Veen E, Tomadin A, Polini M, et al. Optical conductivity of a quantum electron gas in a Sierpinski carpet. Phys Rev B. 2017;96:235438.
[30] Kempkes SN, Slot MR, Freeney SE, et al. Design and characterization of electrons in a fractal geometry. Nat Phys. 2019;15:127–131.
[31] Miniya M, Oubram O, El Hachimi AG, et al. Fano factor in self-similar multibarrier structure based on graphene monolayer. J Appl Phys. 2022;131:024303.
[32] Ugajin R, Hirata S, Kuroki Y. Anderson transition driven by running fractal dimensions in a fractal-shaped structure. Physica A. 2000;278:312–326.
[33] Bernardo C, Moura I, Fernandez YN, et al. Energy transfer via exciton transport in quantum Dot based self-assembled fractal structures. J Phys Chem C. 2014;118:4982–4990.
[34] Ugajin R. Ferromagnetism in fractal-based complexes. J Appl Phys. 2002;92:5772.
[35] Volpe G, Volpe G, Quidant R. Fractal plasmonics: subdiffraction focusing and broadband spectral response by a sierpinski nanocarpet. Opt Expr. 2011;19:3612–3618.
[36] Rasouli Kenari A, Solaimani M. Optical properties of two dimensional fractal shaped nanostructures: comparison of sierpinski triangles and sierpinski carpets. Opt Commun. 2020;474:126185.
[37] Solaimani M, Rasouli Kenari A. A nonparabolic conduction band study of circular quantum dot optical properties: modeling of surface roughness by using Koch snowflakes. J Nanopart Res. 2020;22:242.
[38] Solaimani M. Optical rectification coefficient of GaAs/$Al_xGa_{1-x}As$ Thue–Morse multiple quantum wells. Eur Phys J Plus. 2020;135:455.
[39] Azadi L, Shojaei S. Optical absorption in Thue-Morse and Fibonacci planar graphene superlattices: theoretical report. Phys B. 2019;564:10–16.
[40] Amini M, Soleimani M, Ehsani MH. Electronic and optical properties of GaAs/AlGaAs Fibonacci ordered multiple quantum well systems. Superlattices Microstruct. 2017;112:680–687.
[41] Dickau JJ. Charting trends in the Mandelbrot set & showing their significance for cosmology. Prespacetime Journal. 2016;7:1319–1332.
[42] Mandelbrot BB. The fractal geometry of nature. New York: W.H. Freeman and Company; 1982.
[43] Gardi L. The Mandelbrot set and the fractal nature of light, the universe, and everything. Proc. of SPIE 8832. 2013;883210-1–883210-16.
[44] Beck C. Physical meaning for mandelbrot and Julia sets. Physica D. 1999;125:171–182.
[45] Solaimani M, Aleomraninejad SMA. Optical properties of energy-dependent effective mass GaAs/$Ga_xIn_{1-x}As$ and GaAs/$Al_xGa_{1-x}As$ quantum well systems: a shooting method study. J Electron Mater. 2019;48:942.
[46] Ashrafi-Dalkhani V, Ghajarpour-Nobandegani S, Karimi MJ. Effects of spin–orbit interactions, external fields and eccentricity on the optical absorption of an elliptical quantum ring. Eur Phys J B. 2019;92:19.
[47] Yesilgul U, Ungan F, Kasapoglu E, et al. The linear and nonlinear intersubband optical absorption coefficients and refractive index changes in a V-shaped quantum well under the applied electric and magnetic fields. Superlattices Microstruct. 2011;50:400–410.
[48] Solaimani M. Intersubband optical properties of three electrons confined in multishell quantum dots: comparison of two semiconducting compounds. J Comput Electron. 2018;17:1135–1142.
[49] Adachi S. Gaas, AlAs, and Al_xGa_{1-x} As: material parameters for use in research and device applications. J Appl Phys. 1985;58:R1–R29.

Appendix 1. The effect of the composition parameters *x* on the optical properties of Mandelbrot QDs

Figure A1 presents the variation of the linear absorption coefficient (1/*m*) as a function of the incident photon energy (eV) for different composition parameters $x = 0.05, 0.15, 0.25, 0.35$ and 0.45. It is assumed $L = 300A^0$ and nine Mandelbrot iteration numbers. Here, when the composition parameters *x* increases the absorption amplitude decreases ant its position blueshift and then becomes fixed. The behavior of the absorption peak height agrees with Figure 10C. Also, the mentioned blueshift agrees with Figure 10B. Also, Figure A1B gives the variation of the first five lowest energy eigenvalues as a function of the composition parameter *x* in $Al_xGa_{1-x}As$ semiconductor system. In this figure, by increasing the composition parameter *x* the energy levels increase and then saturate. The electron effective mass and the potential profile change as $m^* = (0.067 + 0.083 * x) * m_0$ and $V_{conf} = 1.1x$ with the composition parameter *x* [49]. Therefore, larger composition parameter *x* is equivalent to deeper quantum wells in the dot regions. Finally, the 2-1 intersubband transition energy increases and then saturate by increasing the composition parameter *x*.

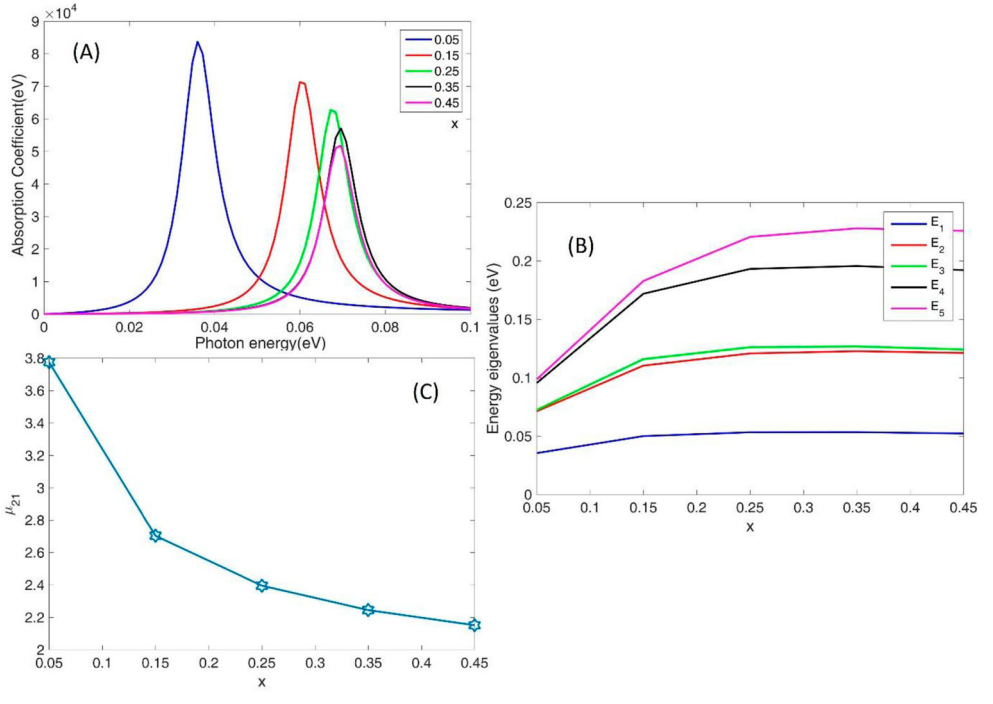

Figure A1. (A) Variation of the linear absorption coefficient (1/*m*) as a function of the incident photon energy (eV) for some composition parameters $x = 0.05, 0.15, 0.25, 0.35$ and 0.45. (B) Variation of the first five lowest energy eigenvalues as a function of the composition parameter *x* in $Al_xGa_{1-x}As$ semiconductor system. (C) Variation of the dipole matrix element μ_{12} as a function of the composition parameters *x*. It is assumed $L = 300A^0$, $m = 2$, and nine Mandelbrot iteration numbers.